ORIGINAL RESEARCH
https://doi.org/10.4209/aaqr.240024

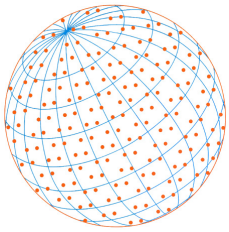

Aerosol and Air Quality Research

Special Issue:
Carbonaceous Aerosols in the Atmosphere (V)

Black Carbon Concentration and Potential Source Regions: A Case Study of the Yellow River Basin in Shandong Province, China

Yuxia Wang[1], Yanni Rong[1], Kai Qu[2], Qing Zhao[1], Yingming Jiang[1], Xiaolei Bao[3*], Yang Wang[4*]

[1] Shandong Agriculture and Engineering University, Jinan 250100, China
[2] Shandong Provincial Eco-environment Monitoring Center, Jinan 250101, China
[3] Hebei Chemical & Pharmaceutical College, Shijiazhuang 050026, China
[4] School of Geographical Sciences, Hebei Normal University, Shijiazhuang 050024, China

ABSTRACT

Black carbon (BC) concentrations and potential source regions were analyzed for nine cities in the Yellow River Basin in Shandong Province from September 2021 to August 2022. Higher BC concentrations were found in Jinan, Tai'an, Jining, and Dezhou, situated in the central part of the study area. BC concentration exhibited the highest values in winter, followed by autumn, spring and summer in all cities excluding Jinan. The monthly average BC concentrations in Jinan ranged from 0.69 to 3.92 μg m^{-3}. BC concentration exhibited a pronounced diurnal variation, which decreased from the morning peak to afternoon. The analysis of related pollutants revealed that BC in Jinan shared similar sources with $PM_{2.5}$ and CO, which were influenced by the distribution of the surrounding high-energy-consuming industries. BC exhibits a correlation of 0.51 and 0.56 with SO_2 and NO_2 in summer, indicating BC is more affected by traffic emissions compared with industrial sources in summer in Jinan. High BC concentration in summer in Jinan is associated with poor diffusion conditions due to terrain and meteorology. High BC concentrations may contribute high land surface temperature (LST) in Jinan during summer. The backward trajectory and potential source regions analysis showed that the potential source area of BC varied considerably in different seasons. In winter and autumn, BC mainly came from local emissions. While in spring and summer, regional transport had equal contribution to BC as local emissions, which cannot be ignored. The findings provide insights for protecting the regional atmospheric environment and promoting high-quality development of the study area.

Keywords: Black carbon, Potential source regions, Meteorological factors, Terrain factors, Yellow River Basin

OPEN ACCESS

Received: January 23, 2024
Revised: May 14, 2024
Accepted: May 20, 2024

* **Corresponding Authors:**
Xiaolei Bao
xlbao.st@gmail.com
Yang Wang
wangyang@hebtu.edu.cn

Publisher:
Taiwan Association for Aerosol Research
ISSN: 1680-8584 print
ISSN: 2071-1409 online

1 INTRODUCTION

Black carbon (BC) is a strong light-absorbing substance known for its significant impact on climate, air quality, and human health (Moosmüller *et al.*, 2009; Hachem *et al.*, 2021). Its capacity to absorb solar radiation substantially elevates local atmospheric temperatures, thereby contributing to overall atmospheric warming (Zhou *et al.*, 2009; Johannes, 2011). Research has indicated that BC ranks as the second-largest contributor to climate warming (Ramanathan and Carmichael, 2008; Li *et al.*, 2021). As a primary component of fine particles ($PM_{2.5}$), BC plays a pivotal role in reducing air visibility and influencing the formation and progression of haze events (Chung and Seinfeld, 2005). Moreover, BC is readily mixed with other pollutant particles in the atmosphere and increases the risk of respiratory, blood, and heart-related diseases when absorbed in the human body (Janssen *et al.*, 2011; Liang *et al.*, 2017).

BC particles typically range in size from 0.01 to 1.0 μm and remain suspended in the atmosphere

for periods ranging from several days to a few weeks. Eventually, they return to Earth's surface through dry and wet atmospheric deposition (Bond *et al.*, 2013). Various studies have indicated that meteorological conditions and the emissions of other pollutants significantly influence BC concentrations. Bhat *et al.* (2017) studied BC concentration variations in Srinagar, northwestern Indian Himalaya, in 2013. Their findings revealed significant negative correlations between BC and wind speed, minimum temperature, and total precipitation. Conversely, nighttime relative humidity showed a positive correlation (Bhat *et al.*, 2017). Kucbel *et al.* (2017) observed a negative correlation between BC concentration and temperature as well as wind speed, and a positive correlation with relative humidity in Ostrava, Czech Republic, during 2012–2014. These findings revealed an important effect of meteorology on BC concentration. Ozdemir *et al.* (2014) analyzed the temporal and spatial characteristics of BC distribution in Istanbul. Their study highlighted that the changes in BC concentration were notably influenced by traffic. Zheng *et al.* (2020) analyzed the changes in BC concentration over 2013 to 2018 in Wuhan using the Kolmogorov-Zurbenk filter and multiple linear regression method. This study revealed that the human efforts rather than meteorological conditions dominated the reduction of BC in 2013–2018 in Wuhan.

In addition to local emissions, the contribution of regional transport to BC concentration cannot be ignored. Zheng *et al.* (2019) analyzed the transmission characteristics of BC between the southern edge of the North China Plain and central China during the winter haze period and proposed a strategy to improve the regional air quality. Zhang *et al.* (2020) investigated the spatial distribution and sources of BC in six major Chinese cities during winter and proposed countermeasures to perform region-wide BC pollution control. Wang *et al.* (2023b) found that local emissions and transport from highly industrialized regions contributed significantly to BC in Shijiazhuang. Deng *et al.*'s (2022) study showed that the surrounding region, southwestern Fujian and eastern Guangdong and Hubei, Hunan and Jiangxi were major sources of BC in Xiamen. Their findings provided a basis for decision-making on the reduction of BC pollution in megacities.

In 2019, the emphasis on ecological protection and high-quality development in the Yellow River Basin (YRB) was elevated to a major national strategy (Ren, 2022). Shandong Province, the main battlefield of ecological environmental protection in the lower Yellow River, is a critical link connecting the Beijing-Tianjin-Hebei (BTH) and Yangtze River Delta (YRD) regions. It plays a pivotal role in regional ecological environmental protection and air pollution control. Currently, few studies have analyzed the pollution characteristics and potential sources of BC in the lower Yellow River region. Based on the strategic background of ecological protection and high-quality development of the YRB, this study took the Shandong section of the YRB as the study area. BC pollution characteristics in different seasons and potential source areas were analyzed. The impacts of emission sources, meteorological factors and ecological factors on BC concentrations were also discussed. This study aims to provide a scientific basis for the improvement of regional air pollution and the high-quality development of the regional ecological environment.

2 MATERIALS AND METHODS

2.1 Sampling Sites and Data Acquisition

This study focuses on nine cities located in the lower reaches of the YRB—Jinan (JN), Dongying (DY), Binzhou (BZ), Zibo (ZB), Dezhou (DZ), Heze (HZ), Tai'an (TA), Jining (JNing), and Liaocheng (LC)—as depicted in Fig. 1. The sites information has been summarized in the Supplement Information Table S1. The Environmental Monitoring Station of Jinan city is located on the campus of Shandong Architecture University (117.1912°E, 36.6865°N) in Jinan city, Shandong Province, which has no significant point source of BC in the surrounding region. The cities in the study area exhibit significant diversity in the distribution of high-energy-consuming industries (Shandong Provincial Bureau of Statistics, 2022). According to the 2021 statistics for Shandong Province, sulfur dioxide (SO_2), nitrogen oxides (NO_x), and particulate matter (PM) emissions from industry and residential emissions account for more than 55% of the province's emissions, and high-energy-consuming industries with high carbon emissions significantly impact the atmospheric environment (Shandong Provincial Bureau of Statistics, 2022). In northwestern Shandong Province, cities like Binzhou, Dongying, and Dezhou are characterized by high industrial energy consumption, particularly in

ORIGINAL RESEARCH
https://doi.org/10.4209/aaqr.240024

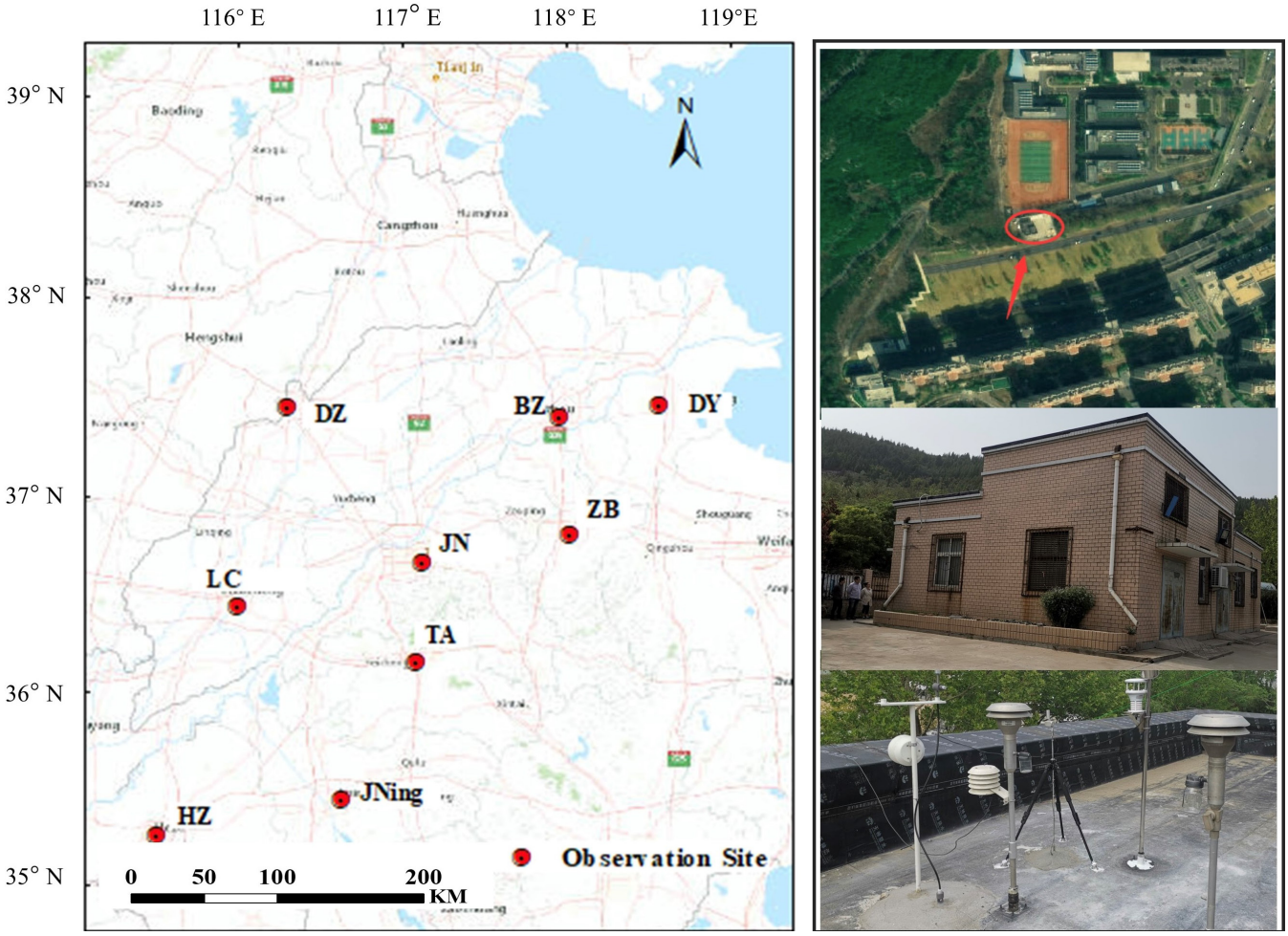

Fig. 1. (a) The distribution of the investigated cities and (b) location of the Jinan observation site and observation instrument.

terms of electric power and heat production, alongside petrochemical processing. High-energy-consuming industries in Zibo are dominated by the petrochemical and coking sectors. In contrast, Jinan shows relatively low industrial energy consumption, but the electric power and heat supply industries consume maximum energy.

In this study, real-time measurements of BC mass concentration were conducted with a seven-wavelength (370, 470, 520, 590, 660, 880, and 950 nm) Aethalometer (AE33, Magee Scientific) from September 1, 2021, to August 31, 2022. AE33 with a $PM_{2.5}$ cut-off inlet was operated at a flow rate of 5 L min^{-1} and used to estimate light attenuation under the principle of optical transmission (Hansen *et al.*, 1984). The concentration measured at 880 nm is considered the standard value of atmospheric BC because BC is the predominant light-absorbing species at this wavelength, with little impact from other compounds (Ganguly *et al.*, 2005). Hourly averages of BC data were computed, and daily and monthly averages were derived from these hourly average data. To ensure data validity, anomalous values and values marked as bad points by the instrument were excluded. During the study period, the atmospheric pollutant data (SO_2, NO_2, CO, and $PM_{2.5}$) and meteorological data (temperature, wind speed, wind direction, and relative humidity) were obtained from hourly data released by the National Environmental Monitoring Platform.

2.2 Land Surface Temperature Analysis

This study employed the series data products of Landsat series with a 30-m spatial resolution from June to August 2022 from the Google Earth Engine (GEE) platform (Huang *et al.*, 2021; Yan *et al.*, 2021). Utilizing remote sensing images, the land surface temperature (LST) was extracted in the study area.

LST can reflect a series of urban heat island effects generated by human activities and emissions of various greenhouse gases (Alexander, 2020). LST is calculated as follows:

$$LST = \frac{T}{1+(\lambda T/\rho)\ln\varepsilon} - 273.15 \quad (1)$$

where T is the brightness temperature observed by the sensor (°C), ε is the surface-specific emissivity, and λ is the center wavelength of the thermal infrared band.

2.3 Backward Trajectory Modeling and Potential Source Area Analysis

To analyze the characteristics of the BC pollutant transport paths and the distribution of potential sources in the study area, backward trajectory analysis, potential source contribution function (PSCF), and concentration weighted trajectory (CWT) analysis were conducted (Wang *et al.*, 2009). The hybrid single-particle Lagrangian integral trajectory model is a widely used air mass trajectory model. In the backward trajectory analysis, the meteorological data used were the Global Data Assimilation System (GDAS) data provided by the National Centers for Environmental Prediction. In addition, 48-h backward trajectories ending at a height of 500 m were calculated using the GDAS reanalysis meteorological dataset with a 0.5° × 0.5° resolution. Trajectory clusters were then obtained from cluster analysis, which was performed based on the inputs of hourly backward trajectories with MeteoInfo software. The simulated paths of the air masses were clustered according to the angle distance algorithm and the mutation points of total spatial variance, and the pollutant concentrations corresponding to the airflow were statistically analyzed in each season (Zhang *et al.*, 2022). The BC concentrations corresponding to the airflow in each season were statistically analyzed.

The PSCF identifies potential air pollutant sources by calculating spatial grid pollution probability (Wang *et al.*, 2023a; Yan *et al.*, 2023). However, there is a large uncertainty in the calculation results when the number of trajectory endpoints within a grid is limited. To reduce uncertainty, this study introduced weighting coefficients and used weighted potential source contribution factor (WPSCF) analysis to assess the potential source areas of BC (Polissar *et al.*, 2001; Liu *et al.*, 2019). Considering seasonal variations in BC concentration, the seasonal average concentrations were set as the thresholds, i.e., 2.0 μg m^{-3} for autumn and winter, 2.5 μg m^{-3} for summer, and 1.0 μg m^{-3} for spring. Trajectories were defined as polluted trajectories if the concentration corresponding to the trajectory exceeded the set threshold (Xu and Akhtar, 2010; Liu *et al.*, 2018).

3 RESULTS AND DISCUSSION

3.1 Spatio-temporal Variation in BC Concentrations

Fig. 2 shows the seasonal BC concentrations in each city. There were large differences in BC concentration among different sites. Central cities like Jinan, Tai'an, Jining, and Dezhou had consistently high BC concentrations. As shown in the statistics columns in Fig. S1, Tai'an showed the highest BC concentration of 3.72 μg m^{-3} than other cities in autumn. Jining showed the highest BC concentration (4.40 μg m^{-3}) among all the cites in winter, followed by Tai'an (4.09 μg m^{-3}) and Dezhou (3.94 μg m^{-3}). In spring, Tai'an (2.32 μg m^{-3}), Dezhou (2.15 μg m^{-3}), and Jining (2.17 μg m^{-3}) reported higher BC concentrations than other cities, while in summer Jinan (2.44 μg m^{-3}) and Tai'an (3.21 μg m^{-3}) had higher BC concentrations among cities. Seasonal changes in BC concentrations in cities excluding Jinan were characterized by the highest in winter, the second highest in autumn and spring, and the lowest in summer, which is consistent with previous research (Zhang *et al.*, 2021).

3.2 Characterization of BC Concentration in Jinan City

In Jinan city, BC concentration peaks with a value of 2.44 μg m^{-3} in summer, followed by autumn (2.03 μg m^{-3}) and winter (1.71 μg m^{-3}), and reached its lowest value in spring (1.01 μg m^{-3}). The mean BC concentration in summer is approximately double of that in spring, which showed great

ORIGINAL RESEARCH
https://doi.org/10.4209/aaqr.240024

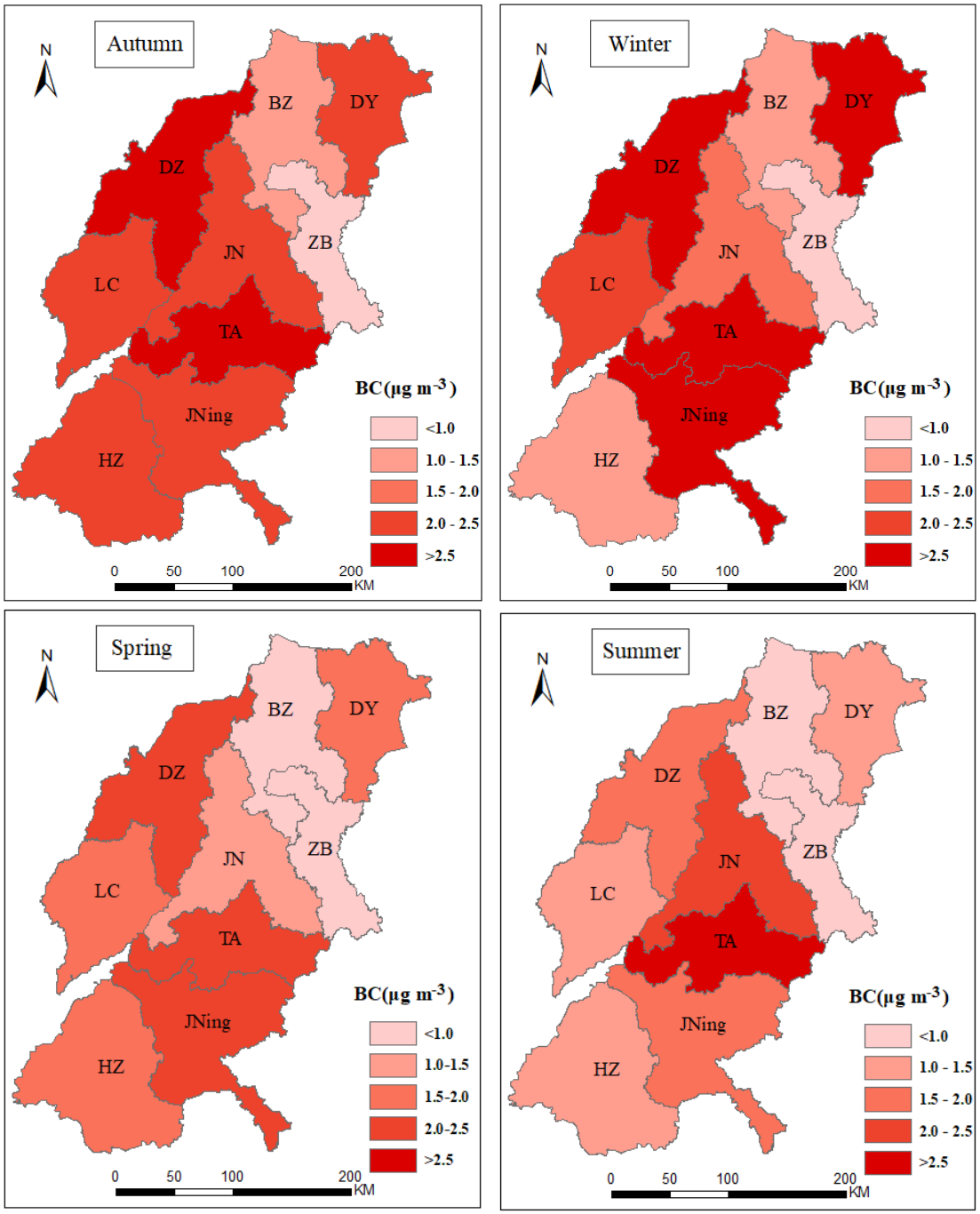

Fig. 2. BC concentrations in the sampling sites in different seasons.

difference with other sites. Analyzing the underlying reasons for this notable spike in BC concentration during summer holds immense importance for improving the overall regional atmospheric environment.

As shown in Fig. 3, the monthly average concentration of BC in Jinan ranged from 0.68 to 3.91 μg m^{-3}, with the lowest value in March and the largest value in August. The daily BC concentration in Jinan during the study period showed a distinct diurnal pattern, increasing steadily before dawn with the major morning peak (2.24 μg m^{-3}) observed around 10:00 in the morning. BC concentration decreased during daytime and reached a diurnal minimum of 1.67 μg m^{-3} at 16:00 in the afternoon. The morning peak was mainly caused by the increased traffic emission during the rush hour. As the decline of the traffic flow and increase of the mixing layer height, BC concentration

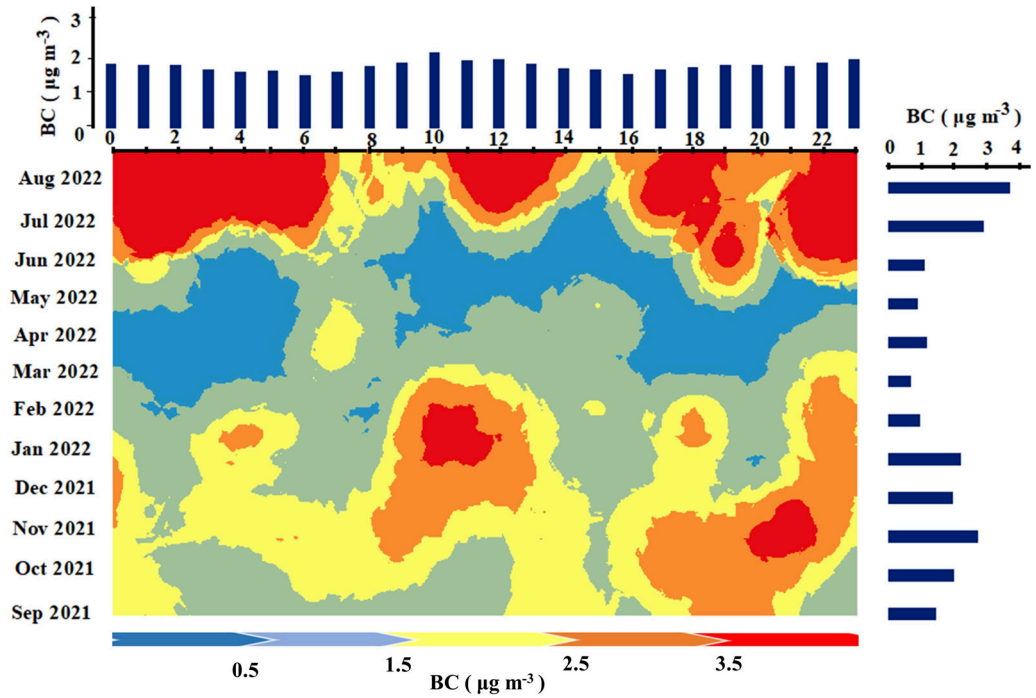

Fig. 3. Monthly and diurnal variations of BC concentration in Jinan.

began to decrease in the afternoon. Afterward, BC concentrations increased again due to the evening traffic rush hour and lower mixing layer height. BC concentrations are typically influenced by a blend of emissions from various sources, meteorological conditions, and atmospheric boundary layer dynamics (Zhao *et al.*, 2012; Liñán-Abanto *et al.*, 2021). To investigate the underlying causes contributing to the elevated BC concentration during summer, the subsequent sections will discuss the effect of emission sources, terrain, and meteorological factors on BC concentration in Jinan.

3.2.1 BC concentrations in relation to emission sources

This section aimed to identify the primary BC emission sources in Jinan through a statistical analysis between BC, SO_2, NO_2, CO, and $PM_{2.5}$ (as showed in Fig. 4 and Table S2). BC exhibited strong associations with CO and $PM_{2.5}$, with correlation coefficient values of 0.73, indicating similar emission sources of BC with CO and $PM_{2.5}$. Typically, SO_2 and NO_2 can be used as indicators of industrial and traffic emissions, respectively. BC exhibits a distinct positive correlation with SO_2, with the highest correlation observed in winter (0.75) and the lowest correlation in summer (0.51), indicating a significant industrial contribution to BC concentrations in Jinan. This indicates the BC concentration in Jinan city may mainly generated from energy-consuming industries, particularly those emitting SO_2. There are 6 industrial parks within 20 km of the monitoring site, mainly consisting of petrochemical, steel, and biomedical enterprises, such as Huangtai power plant and Jinan steelworks. The correlation coefficients between BC and NO_2 in summer (0.56) is lower next to that in winter (0.64) and higher than that in autumn (0.48) and spring (0.39), suggesting, BC in summer is more affected by traffic emissions compared with industrial sources in Jinan.

3.2.2 BC concentration in relation to terrain and meteorological factors

Anthropogenic emission and meteorology are considered as two fundamental factors that determine the variation of aerosol pollution (Tie *et al.*, 2013, 2015). As shown in Fig. 5, the terrain of Jinan is high in the south and low in the north, with an altitude difference of 400 meters. The urban area is like a "shallow-dish", surrounded by mountains in the north, east and south. Under the adverse weather conditions, pollutants tend to accumulate in the "shallow-dish" area, resulting in the accumulation of pollutants and deterioration of urban air quality. The diffusion conditions

ORIGINAL RESEARCH
https://doi.org/10.4209/aaqr.240024

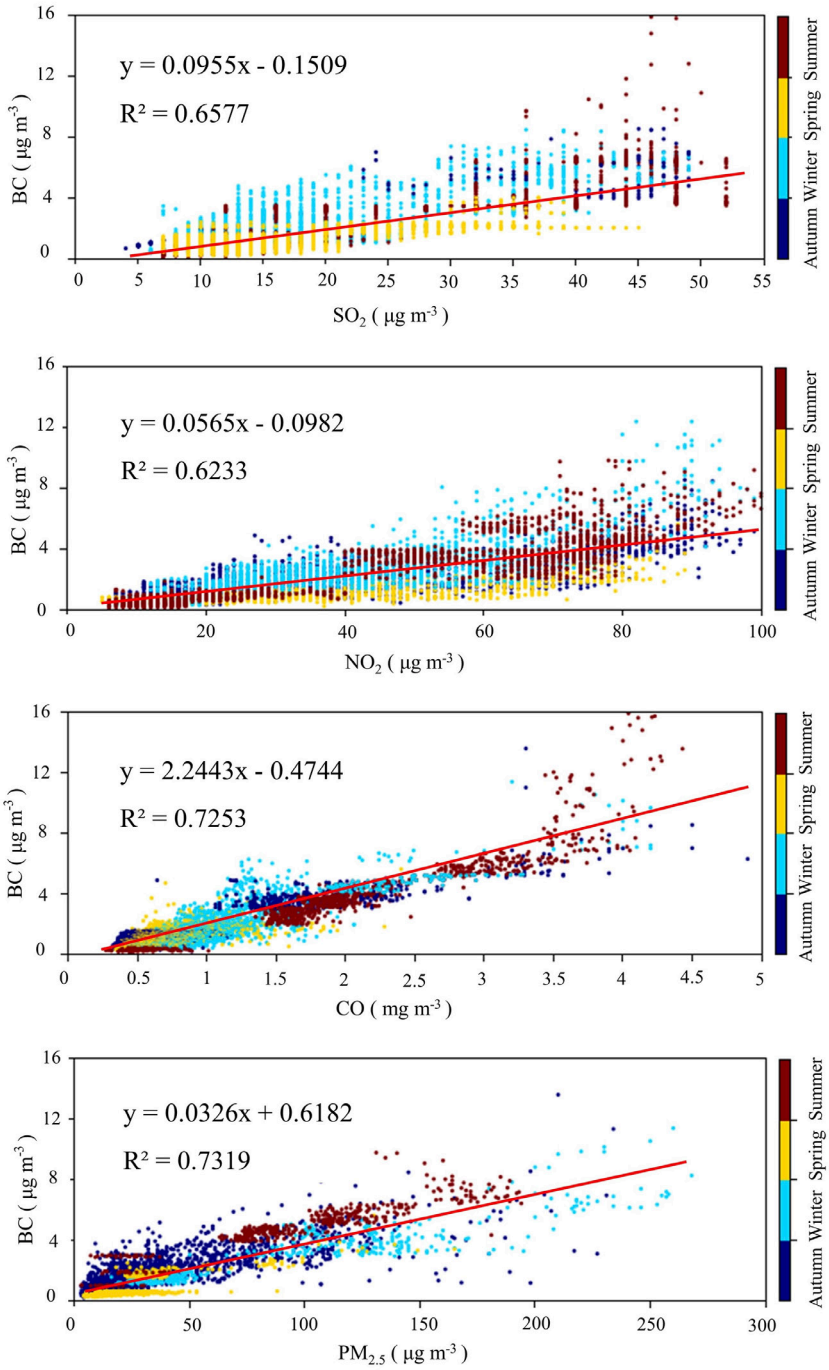

Fig. 4. Correlation between BC and other pollutants.

of Jinan are generally poor, the northern part of the city has better diffusion conditions, and the southwestern and southeastern mountain areas have relative poor diffusion areas. The diffusion conditions are even worse in the central part of the city. In the area with poor diffusion conditions, influenced by mountains in the south, a small wind center is easy to form near the ground in the urban area, which affects the horizontal diffusion of pollutants.

As shown in the Fig. S2, summer recorded the highest average temperature (28°C), and the highest average relative humidity (60%) among the four seasons. Spring showed the highest average wind speed of 3.1 m s^{-1}, with lower relative humidity (40%), resulting in a relatively dry atmospheric condition. The relative humidity in winter and autumn was 45% and 55%, and the wind speed was 2.07 m s^{-1} and 2.0 m s^{-1}, respectively.

ORIGINAL RESEARCH
https://doi.org/10.4209/aaqr.240024

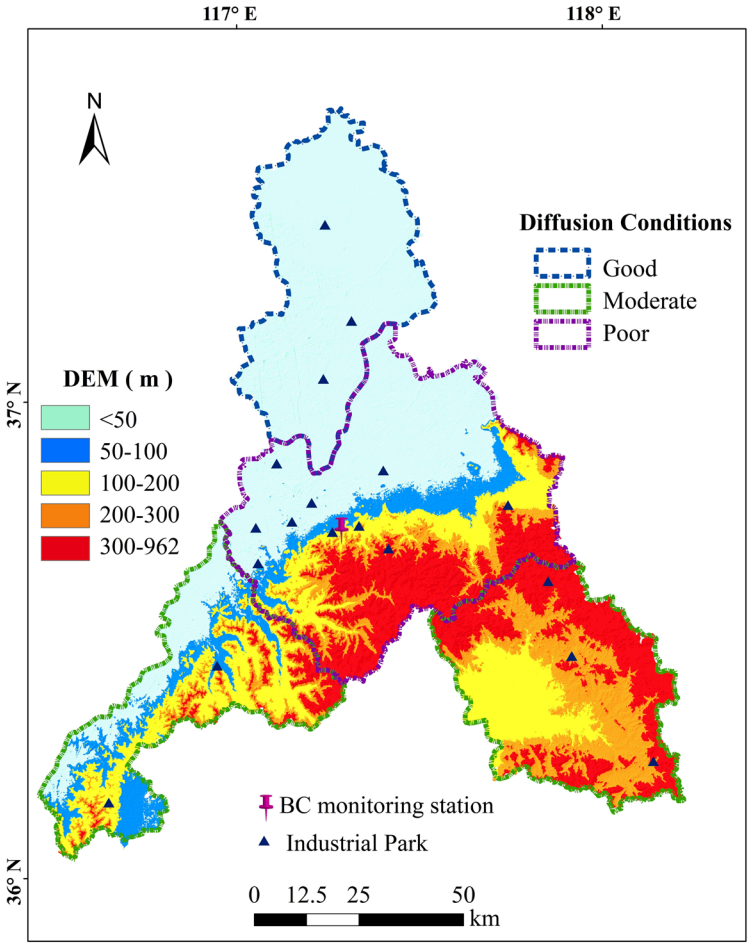

Fig. 5. DEM and industrial park in Jinan. The dotted lines with various colors show the different diffusion conditions, and the purple pinpoint shows the location of Jinan site.

To assess the impact of wind speed and direction on BC concentration values, this study analyzed the correlation between BC concentration and these factors in Jinan during the study period, utilizing SPSS and MeteoInfo software (Fig. 6). The frequency of wind speed less than 2 m s^{-1} was 64.5%, indicating that the city was mostly characterized by static wind and light wind during the observation period. The BC concentration is relatively low when the wind speed is greater than 4 m s^{-1}, when the wind speed is greater than 6 m s^{-1}, BC concentration is 1.11 μg m^{-3}. Contrarily, the BC concentration is much higher when the wind speed is less than 2 m s^{-1}. The average BC concentration was 1.9 μg m^{-3} when the wind speed was between 1 and 2 m s^{-1}, 2.26 μg m^{-3} when the wind speed was less than 1.0 m s^{-1}. The correlation coefficient of BC and monthly mean wind speed data shows that the correlation coefficient is –0.55, indicating that the wind speed is negatively correlated with BC concentration. The monthly mean wind speed in summer (1.85–2.50 m s^{-1}) is close to that in autumn (1.97–2.05 m s^{-1}) and winter (1.88–2.13 m s^{-1}) and significantly lowers than that in spring (2.66–3.12 m s^{-1}). Lower wind speeds hindered the effective dispersion of pollutants, leading to a poor diffusion conditions and the accumulation of BC. The low wind speed in summer may be one of the reasons for the high BC concentration in Jinan.

In terms of wind direction, there was no significant difference in wind frequency in each direction. In autumn, the wind containing high BC concentration is mainly from southeast. In winter, the frequency of wind from northeast is higher but the BC concentration is lower, and the high BC concentration wind mainly comes from the north and northwest. In spring, the wind speed is higher and the frequency of wind from south is the highest, which makes BC present a lower concentration. Wind speeds were lower in summer, and winds from the northeast and the northwest contained higher BC concentrations.

ORIGINAL RESEARCH
https://doi.org/10.4209/aaqr.240024

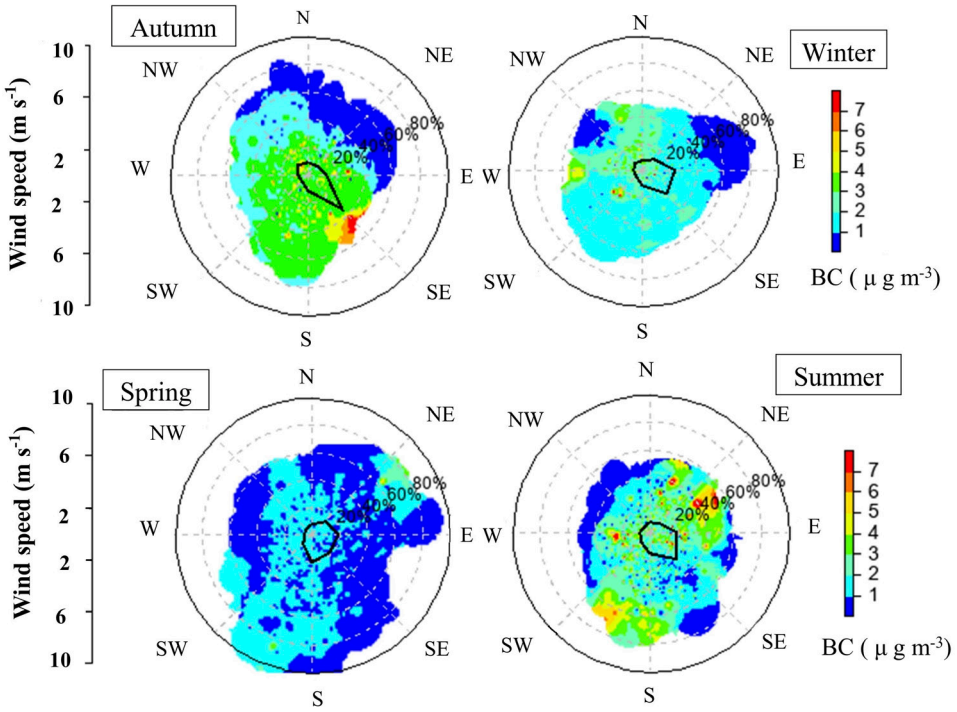

Fig. 6. Relationship between BC concentration and winds during the study period.

In summer, the prevailing winds coming from east, south and northeast are blocked, resulting in unfavorable diffusion conditions. In addition, a large number of industrial parks are distributed in area with poor diffusion conditions (Fig. 5). This makes it easy for pollutants to accumulate in the foothills, presenting a high BC concentration in summer in Jinan. Therefore, in the urban environment planning, industrial parks and key emissions sources should be built in areas with good diffusion conditions.

Previous studies also suggest that planetary boundary layer height (PBLH) is major meteorological parameters in controlling the variability of BC concentration in megacities. These studies find that lower PBLH confine aerosols near the surface and produce high BC concentrations (Liu *et al.*, 2013; Zhao *et al.*, 2013; He *et al.*, 2015). Since no PBLH data was obtained during the study period, the effect of PBLH on BC concentrations was not included in this paper.

3.3 Transport Pathways of BC

Seasonal clusters of backward trajectories obtained by the HYSPLIT model with the average BC contributions are illustrated in Fig. 7. Mean concentrations of BC of each cluster in different seasons are summarized in Table 1. It is clearly shown that origins and transport pathways of air masses arriving in Jinan exhibited distinct seasonal variations.

In autumn, trajectory 2, originating from Mongolia and traveling through Inner Mongolia, Datong, Shanxi, Shijiazhuang, Hengshui, and Dezhou, constituted the primary proportion of the airflow and pollutant trajectories, accounting for 34.03% and 41.66%, respectively. The BC concentration in the pollutant trajectory was 3.09 μg m^{-3}. Trajectory 1, primarily short-range transmission airflow, reached Jinan through Zaozhuang, Linyi, and Tai'an in the southern region of Shandong Province. Its airflow and pollutant trajectories accounted for 31.93% and 38.88% of the total trajectories, respectively. Trajectory 4 originated from Inner Mongolia and Chifeng and passed through Qinhuangdao, Dongying, Binzhou, and Zibo before reaching Jinan city. This trajectory accounted for 33.19% of the airflow trajectory, with an average BC concentration of 2.28 μg m^{-3}. The associated pollutant trajectory accounted for 19.46%, exhibiting a pollutant concentration of 4.08 μg m^{-3}. Trajectory 3, originating from Russia and passing through Mongolia, represents long-distance transport airflow. Its percentages in the pollutant trajectories were the lowest, suggesting relatively cleaner airflow conditions.

ORIGINAL RESEARCH
https://doi.org/10.4209/aaqr.240024

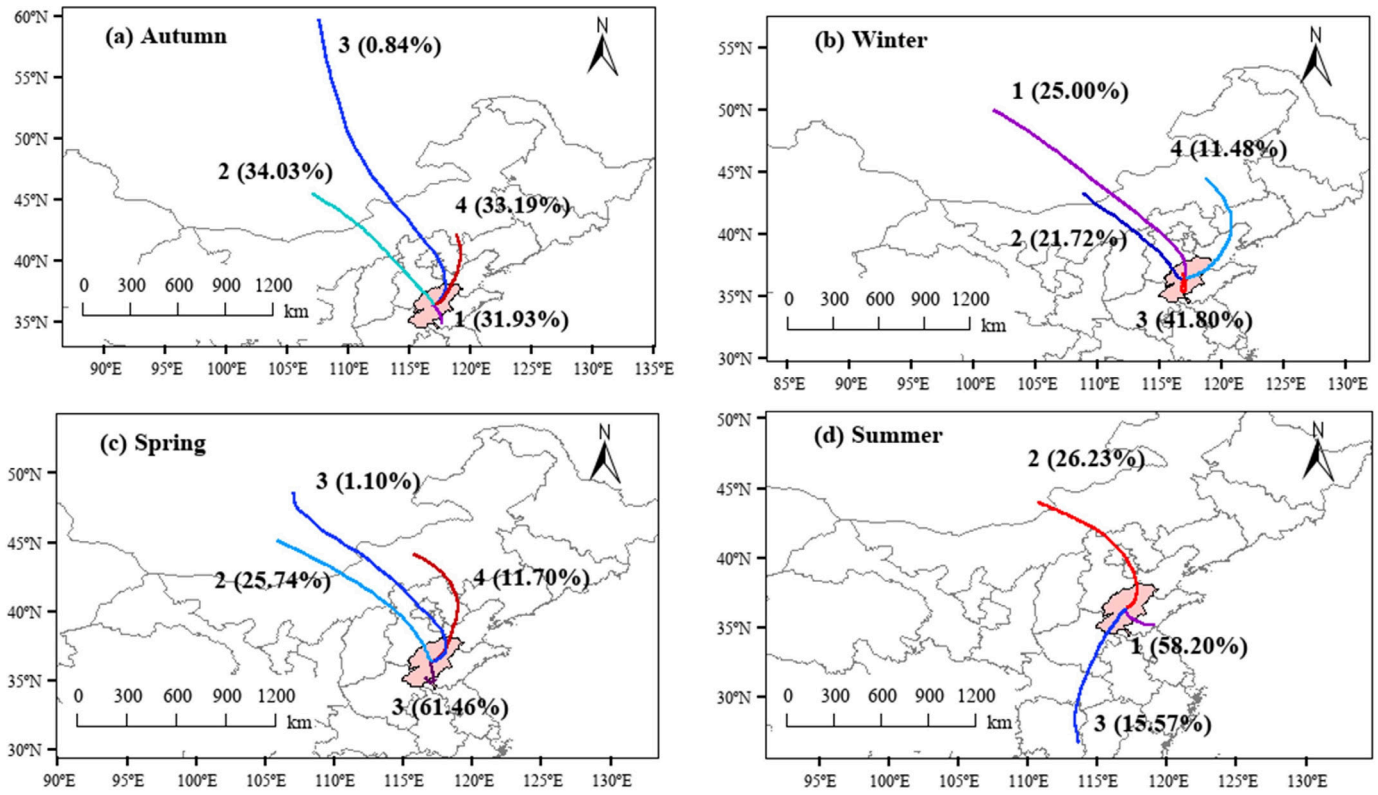

Fig. 7. Backward trajectory clusters in different seasons in Jinan.

Table 1. Percentage and mean concentrations of BC of each cluster in different seasons.

Season	Cluster	All trajectories		Pollution trajectories	
		Percentage (%)	BC concentration (μg m^{-3})	Percentage (%)	BC concentration (μg m^{-3})
Autumn	1	31.93%	2.99	38.88%	3.71
	2	34.03%	2.09	41.66%	3.09
	3	0.85%	0.52	–	–
	4	33.19%	2.28	19.46%	4.08
Winter	1	25.00%	1.78	9.23%	3.52
	2	21.72%	2.86	75.38%	3.61
	3	41.80%	2.22	6.16%	5.23
	4	11.48%	1.78	9.23%	2.87
Spring	1	61.46%	1.16	82.58%	1.47
	2	25.74%	0.72	9.81%	1.42
	3	1.10%	0.67	0.33%	1.17
	4	11.70%	0.86	7.28%	1.50
Summer	1	58.20%	3.71	52.6%	5.18
	2	26.23%	4.24	33.3%	5.47
	3	25.57%	3.81	14.1%	5.87

In winter, trajectory 3, originating from the central region of Shandong Province, including Jining and Tai'an, represents a short-distance transport air mass, accounting for 41.8% of the airflow trajectory and with a BC concentration of 2.22 μg m^{-3}. The mountainous terrain in this area tended to obstruct airflow, hampering pollutant diffusion and thus resulting in higher BC concentrations. Two airflow trajectories originated from the Inner Mongolia region. Trajectory 2 traversed Datong city and Shijiazhuang, reaching Jinan via Dezhou. Its pollutant trajectory accounted for 75.38% of

the total trajectories, which is significantly higher than the proportion of other trajectory clusters. The BC pollution concentration of trajectory 2 is 3.61 μg m^{-3}, making it the primary pollution trajectory in winter. The longer and faster airflow transportation path of trajectory 1 facilitated better diffusion, leading to decreased concentration along its route. This comparatively lower BC concentration in trajectory 1 indicates improved atmospheric environmental quality in the BTH region. The lower average BC concentration in trajectory 4 originated from Inner Mongolia and passed through Bohai had the lowest BC concentration.

In spring, trajectory 1 originated from Jining, Zaozhuang, and Tai'an, representing a short-range transport air mass. This trajectory exhibited the highest probability of airflow (61.46%) and the most significant portion of the pollution trajectory (82.58%). Trajectory 1 was the primary pollution trajectory in spring with a mean BC concentration of 1.16 μg m^{-3}. Additionally, two long-distance transport airflows originated from Mongolia during this season. Trajectory 2 traversed through Inner Mongolia, Datong, Baoding, Hengshui, and Dezhou. This trajectory accounted for a relatively large proportion of air mass trajectories (25.74%) and pollution trajectories (9.81%). However, BC concentration of this trajectory was low (0.72 μg m^{-3}).

In summer, trajectory 1 originated from central Jiangsu Province, passing through Xuzhou, Linyi, Jining, and Tai'an had the largest proportion. Trajectory 2 originated from Mongolia, traversing central Inner Mongolia, Hebei, Beijing, and Tianjin before arriving in Jinan. This trajectory cluster accounted for 26.23% of the total trajectory and 33.3% of the pollution trajectory, with the highest concentration of 4.24 μg m^{-3}. Trajectory 3 represented long-distance transport airflow and originated from the eastern part of Hunan Province, passing through Changsha, Yueyang, Xinyang, Shangqiu, Heze, Jining, and Tai'an. Although the pollution trajectory accounted for a relatively low value of 14.1%, its BC concentration value was the highest (5.87 μg m^{-3}).

In summary, the prevailing air masses during autumn and winter predominantly came from the north and northwest, constituting 67% and 45% of the total trajectories, respectively, correlating with higher BC concentrations. In spring, air masses primarily from the south, accounting for 61% of the total trajectories, with the highest BC concentration of 1.47 μg m^{-3}. In summer, the prevailing air masses came predominantly from the southeast, accounted for 58% of the total trajectories, with a BC concentrations of 5.18 μg m^{-3}.

3.4 Potential Source Areas of BC

BC potential source areas were also analyzed by computing WPSCF values in this study. According to the geographical radius of Jinan city (i.e., 200 km), the potential source areas were divided into two categories as divided by a 200-km radius centered at the observation site (the smaller circle in Fig. 8 and Fig. 9). Consequently, the area within the 200 km radius represents the contribution of local sources, with the other areas corresponding to regional transport. Areas where the WPSCF exceeded 0.6 were identified as significant potential sources of BC pollution. Fig. 8 illustrates the pronounced seasonal variations in these potential BC source areas.

The autumn season revealed a significant potential pollution source area for BC, which is prominently found in Liaoning, Hebei, and Inner Mongolia. Hebei, Shanxi, and Inner Mongolia, particularly Datong in Shanxi, appeared to be primary potential pollution sources. These regions, according to China's Energy Statistics Yearbook, serve as major industrial hubs, exhibiting considerable energy consumption and high pollutant emissions. In winter, the potential BC source areas were concentrated mainly within Shandong Province, with higher values in Weifang, Rizhao, Dongying, and Zibo. Spring showed a more dispersed pattern in BC potential source areas, prominently located around the borders of Hebei and Liaoning, as well as Shanxi and Henan, and the eastern region of Shandong Province. Summer illustrates a widespread distribution of BC potential sources encompassing local regions in Shandong Province, along with Henan and Hunan provinces.

The concentration weighting trajectory (CWT) analysis was conducted to further investigate the potential source areas' contribution to BC pollution in the study area. The WCWT values signify the magnitude of contribution of a potential source area to the study site. Based on the distinct BC concentration patterns observed in different seasons, the major contributing areas were identified according to the WCWT values exceeding specific thresholds: that is values 1.0 μg m^{-3} in spring, 3 μg m^{-3} in autumn and winter, and 5 μg m^{-3} in summer.

ORIGINAL RESEARCH
https://doi.org/10.4209/aaqr.240024

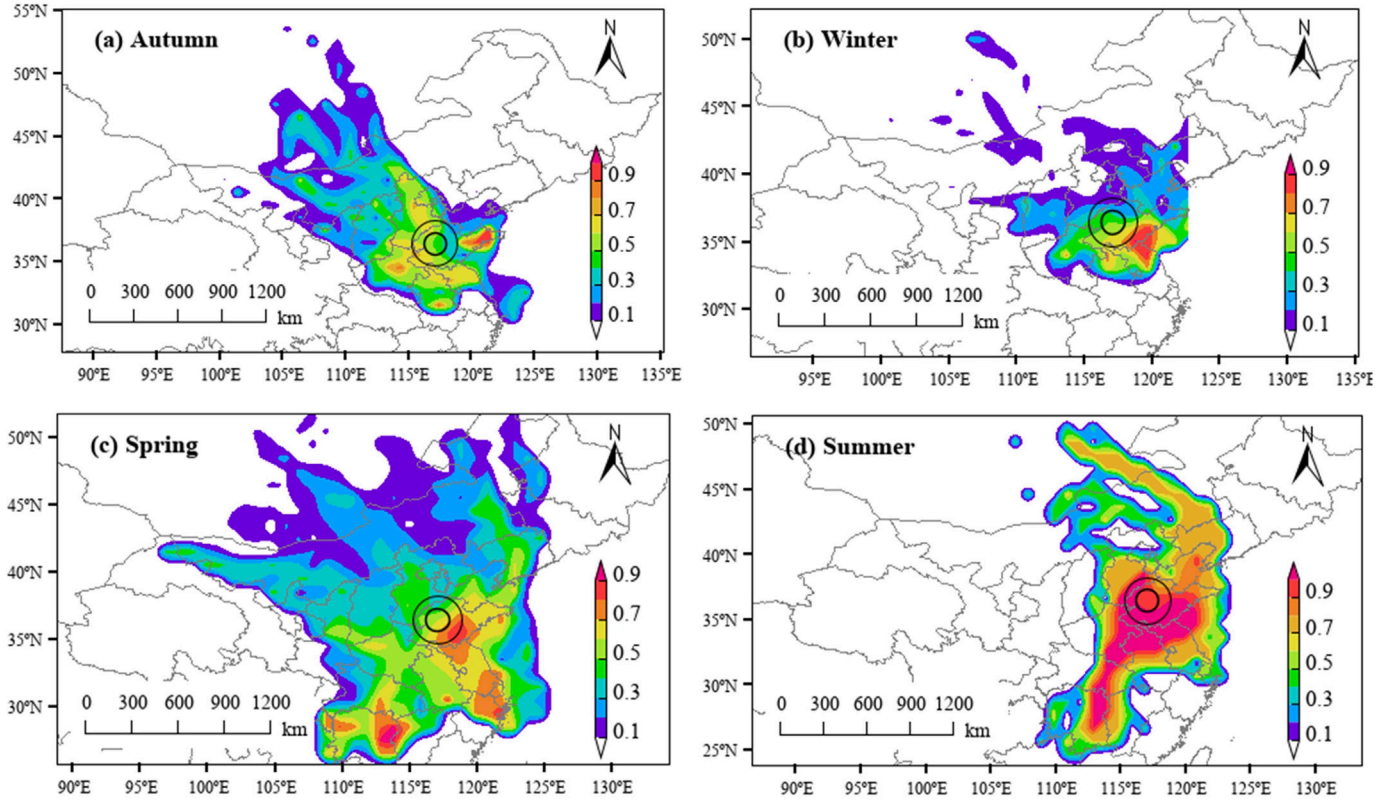

Fig. 8. WPSCF maps of BC in four seasons.

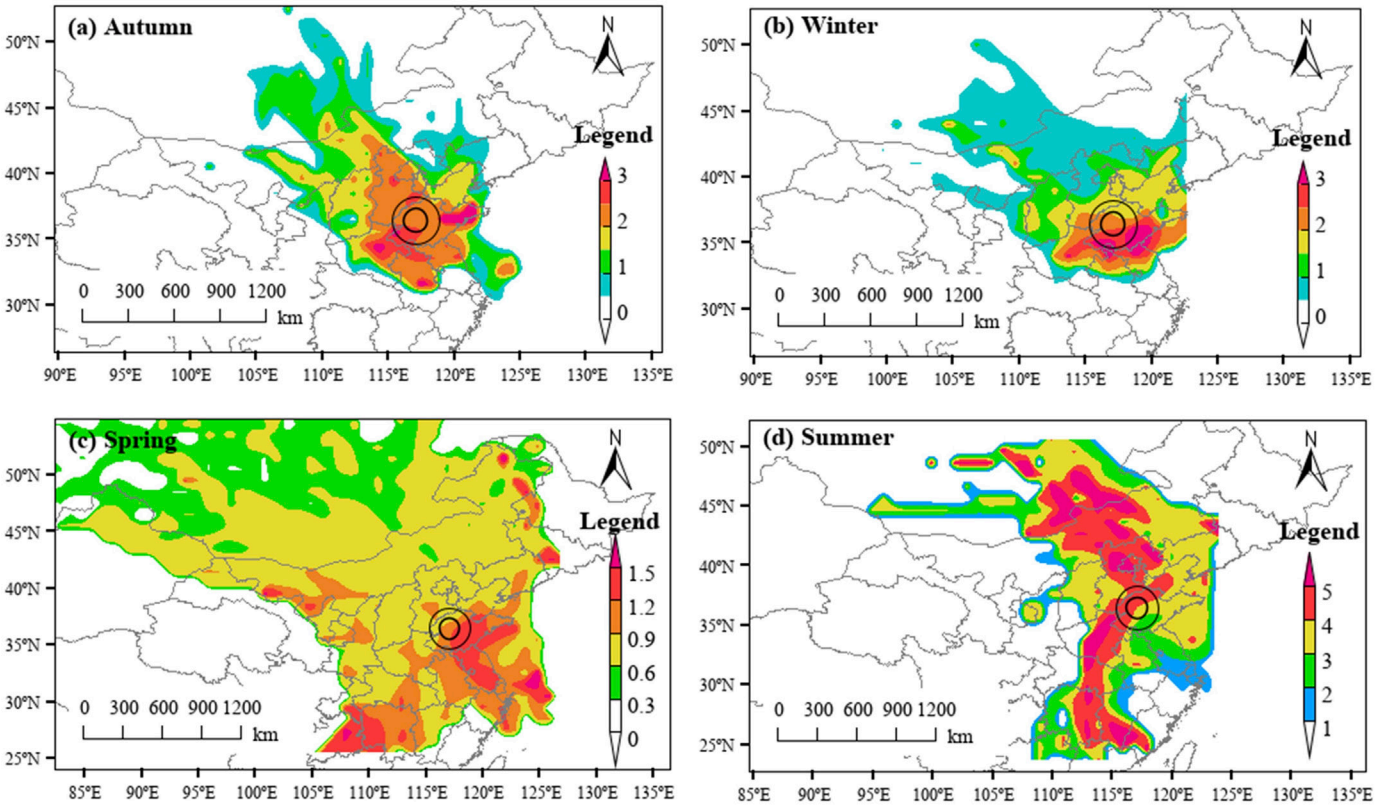

Fig. 9. WCWT maps of BC in four seasons.

ORIGINAL RESEARCH
https://doi.org/10.4209/aaqr.240024

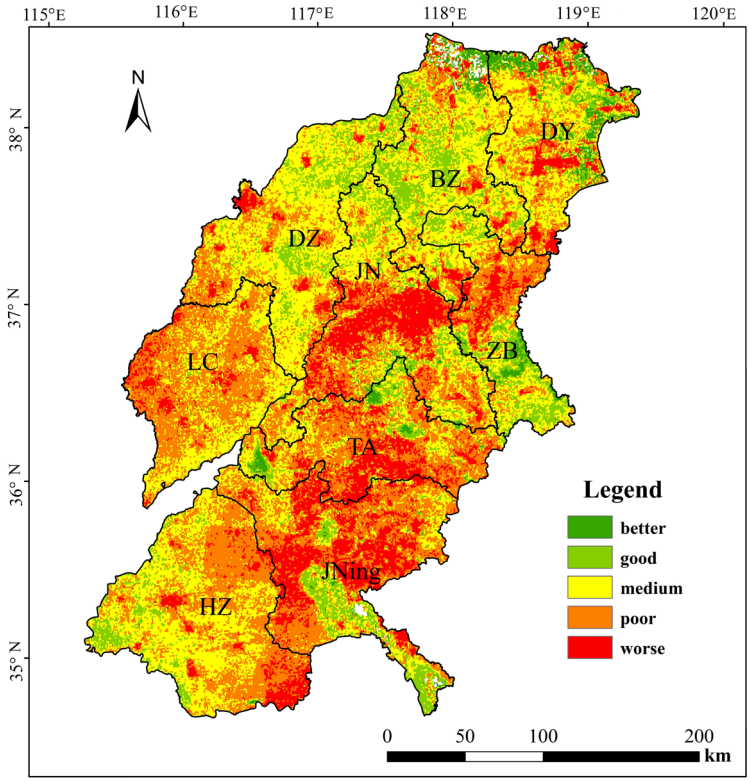

Fig. 10. LST of the study area.

The WCWT results are showed in Fig. 9. In autumn, the regions with high WCWT values (> 3 μg m^{-3}) were mainly distributed in Shandong Peninsula, Hebei and Henan. While in winter, the regions with high WCWT values (> 3 μg m^{-3}) were mainly distributed in eastern Shandong. The regions with high WCWT values (>1.0 μg m^{-3}) in spring located in eastern Shandong and its neighboring provinces (Jiangsu and Henan). The ranges of regions with high WCWT values (> 5 μg m^{-3}) in summer were significantly larger than other seasons, which may contribute to the high BC concentration in Jinan in summer. Controlling BC emissions in these areas will reduce BC concentrations, which may reduce the LST in summer in Jinan.

3.5 Impact of BC Concentrations on the LST

LST can be used to reflect the land surface temperature. To investigate the impact of BC concentration on regional climate in summer in Jinan, this study computed the LST values of the study area during the observation period. As shown in Fig. 10, the LST exhibited obvious difference between different sites. As a result, Jinan exhibited a positive correlation of 0.87 between BC concentrations and LST in summer. BC has the ability to absorb almost the entire solar spectrum, making it an important greenhouse effect species in the atmosphere. The higher BC concentration in summer may contribute the higher land surface temperature in Jinan.

4 CONCLUSIONS

This study reported the BC concentration in nine cites in the Yellow River Basin in Shandong Province from September 2021 to August 2022. Characteristics of BC concentration, transport paths and the distribution of major potential source areas were analyzed. The effects of emission sources, meteorological factors and ecological factors on BC concentrations were discussed. The main conclusions are as follows:

(1) Central cities such as Jinan, Tai'an, Jining, and Dezhou exhibited higher BC concentration values during the study period. Seasonal changes in BC concentrations excluding Jinan were

characterized by the highest in winter, the second highest in autumn and spring, and the lowest in summer. However Jinan city showed the highest BC concentration in summer, which is double of that in spring. The higher BC concentration in summer may contribute the higher LST in Jinan.

(2) High BC concentration in summer in Jinan is affected by the terrain and wind. The Prevailing winds coming from east, south and northeast in summer in Jinan are blocked, resulting in unfavorable diffusion conditions and making it easy for pollutants to accumulate in the urban area. In winter and autumn, BC aerosols in Jinan mainly came from local emissions, while in spring and summer, regional transport had equal contribution to BC as local emissions, which cannot be ignored.

(3) PSCF analysis showed that Shandong, Henan, Hebei were identified as the major potential source regions to the study area. It is noteworthy that the ranges of regions with high WCWT values (> 5 μg m^{-3}) in summer were significantly larger than other seasons. The Yellow River basin is an important ecological barrier and is strategically significant for China's eco-environment and development. Therefore, further research will be conducted on long-term and wide-range BC monitoring on this region, in order to provide scientific basis for improving regional atmospheric environment and climate.

ACKNOWLEDGMENTS

This research was funded by the Jinan philosophy and social science project: Study on the coordination between ecological quality protection and high-quality development in the yellow river basin of Shandong province (Grant No. JNSK22C12), Quality monitoring and database construction of cultivated land resources (Grant No. SGYHX2023-39), Hebei Technological Innovation Center for Volatile Organic Compounds Detection and Treatment in Chemical Industry (Grant No. ZXJJ20210406) and National Natural Science Foundation of China (Grant No. 42205131).

ADDITIONAL INFORMATION AND DECLARATIONS

Disclaimer

The authors declare that they have no known competing financial interests or personal relationships that could have appeared to influence the work reported in this paper.

Supplementary Material

Supplementary material for this article can be found in the online version at https://doi.org/10.4209/aaqr.240024

REFERENCES

Alexander, C. (2020). Normalised difference spectral indices and urban land cover as indicators of land surface temperature (LST). Int. J. Appl. Earth Obs. Geoinf. 86, 102013. https://doi.org/10.1016/j.jag.2019.102013

Bhat, M.A., Romshoo, S.A., Beig, G. (2017). Aerosol black carbon at an urban site-Srinagar, Northwestern Himalaya, India: Seasonality, sources, meteorology and radiative forcing. Atmos. Environ. 165, 336–348. https://doi.org/10.1016/j.atmosenv.2017.07.004

Bond, T.C., Doherty, S.J., Fahey, D.W., Forster, P.M., Berntsen, T., DeAngelo, B.J., Flanner, M.G., Ghan, S., Kärcher, B., Koch, D., Kinne, S., Kondo, Y., Quinn, P.K., Sarofim, M.C., Schultz, M.G., Schulz, M., Venkataraman, C., Zhang, H., Zhang, S., Bellouin, N., *et al.* (2013). Bounding the role of black carbon in the climate system: A scientific assessment. J. Geophys. Res. 118, 5380–5552. https://doi.org/10.1002/jgrd.50171

Chung, S.H., Seinfeld, J.H. (2005). Climate response of direct radiative forcing of anthropogenic black carbon. J. Geophys. Res. 110, 2004JD005441. https://doi.org/10.1029/2004JD005441

Deng, J., Zhao, W., Wu, L., Hu, W., Ren, L., Wang, X., Fu, P. (2020). Black carbon in Xiamen, China:

Temporal variations, transport pathways and impacts of synoptic circulation. Chemosphere 241, 125–133. https://doi.org/10.1016/j.chemosphere.2019.125133

Ganguly, D., Jayaraman, A., Gadhavi, H., Rajesh, T.A. (2005). Features in wavelength dependence of aerosol absorption observed over central India. Geophys. Res. Lett. 32, 2005GL023023. https://doi.org/10.1029/2005GL023023

Hachem, M., Loizeau, M., Saleh, N., Momas, I., Bensefa-Colas, L. (2021). Short-term association of in-vehicle ultrafine particles and black carbon concentrations with respiratory health in Parisian taxi drivers. Environ. Int. 147, 106346. https://doi.org/10.1016/j.envint.2020.106346

Hansen, A.D.A., Rosen, H., Novakov, T. (1984). The aethalometer — An instrument for the real-time measurement of optical absorption by aerosol particles. Sci. Total Environ. 36, 191–196. https://doi.org/10.1016/0048-9697(84)90265-1

He, H., Tie, X., Zhang, Q., Liu, X., Gao, Q., Li, X., Gao, Y. (2015). Analysis of the causes of heavy aerosol pollution in Beijing, China: A case study with the WRF-Chem model. Particuology 20, 32–40. https://doi.org/10.1016/j.partic.2014.06.004

Huang, H., Chen, W., Zhang, Y., Qiao, L., Du, Y. (2021). Analysis of ecological quality in Lhasa Metropolitan Area during 1990–2017 based on remote sensing and Google Earth Engine platform. J. Geogr. Sci 31, 265–280. https://doi.org/10.1007/S11442-021-1846-8

Janssen, N.A.H., Hoek, G., Simic-Lawson, M., Fischer, P., Bree, L.v., Brink, H.t., Keuken, M., Atkinson, R.W., Anderson, H.R., Brunekreef, B., Cassee, F.R. (2011). Black carbon as an additional indicator of the adverse health effects of airborne particles compared with PM_{10} and $PM_{2.5}$. Environ. Health Perspect. 119, 1691–1699. https://doi.org/10.1289/ehp.1003369

Johannes, Q. (2011). Global warming: The soot factor. Nature 471, 456–457. https://doi.org/10.1038/471456a

Kucbel, M., Corsaro, A., Švédová, B., Raclavská, H., Raclavský, K., Juchelková, D. (2017). Temporal and seasonal variations of black carbon in a highly polluted European city: Apportionment of potential sources and the effect of meteorological conditions. J. Environ. Manage. 203, 1178–1189. https://doi.org/10.1016/j.jenvman.2017.05.038

Li, H., Huang, K., Fu, Q., Lin, Y., Chen, J., Congrui, Tian, X., Tang, Q., Song, Q., Wei, Z. (2021). Airborne black carbon variations during the COVID-19 lockdown in the Yangtze River Delta megacities suggest actions to curb global warming. Environ. Chem. Lett. 20, 71–80. https://doi.org/10.1007/S10311-021-01327-3

Liang, F., Tian, L., Guo, Q., Westerdahl, D., Liu, Y., Jin, X., Li, G., Pan, X. (2017). Associations of $PM_{2.5}$ and black carbon with hospital emergency room visits during heavy haze events: A case study in Beijing, China. Int. J. Environ. Res. Public Health 14, 725. https://doi.org/10.3390/ijerph14070725

Liñán-Abanto, R.N., Salcedo, D., Arnott, P., Paredes-Miranda, G., Grutter, M., Peralta, O., Carabali, G., Serrano-Silva, N., Ruiz-Suárez, L.G., Castro, T. (2021). Temporal variations of black carbon, carbon monoxide, and carbon dioxide in Mexico City: Mutual correlations and evaluation of emissions inventories. Urban Clim 37, 100855. https://doi.org/10.1016/J.UCLIM.2021.100855

Liu, C., Cong, H., Zhang, H., Zhang, B., Wang, G., Zhu, W., Xu, R. (2019). A severe fog-haze episode in Beijing-Tianjin-Hebei region: Characteristics, sources and impacts of boundary layer structure. Atmos. Pollut. Res. 10, 1190–1202. https://doi.org/10.1016/j.apr.2019.02.002

Liu, S., Hua, S., Wang, K., Qiu, P., Liu, H., Wu, B., Shao, P., Liu, X., Wu, Y., Xue, Y., Hao, Y., Tian, H. (2018). Spatial-temporal variation characteristics of air pollution in Henan of China: Localized emission inventory, WRF/Chem simulations and potential source contribution analysis. Sci. Total Environ. 624, 396–406. https://doi.org/10.1016/j.scitotenv.2017.12.102

Liu, X.G., Li, J., Qu, Y., Han, T., Hou, L., Gu, J., Chen, C., Yang, Y., Liu, X., Yang, T., Zhang, Y., Tian, H., Hu, M. (2013). Formation and evolution mechanism of regional haze: a case study in the megacity Beijing, China. Atmos. Chem. Phys. 13, 4501–4514. https://doi.org/10.5194/acp-13-4501-2013

Moosmüller, H., Chakrabarty, R.K., Arnott, W.P. (2009). Aerosol light absorption and its measurement: A review. J. Quant. Spectrosc. Radiat. Transfer 110, 844–878. https://doi.org/10.1016/j.jqsrt.2009.02.035

Ozdemir, H., Pozzoli, L., Kindap, T., Demir, G., Mertoglu, B., Mihalopoulos, N., Theodosi, C., Kanakidou, M., Im, U., Unal, A. (2014). Spatial and temporal analysis of black carbon aerosols

in Istanbul megacity. Sci. Total Environ. 473–474, 451–458. https://doi.org/10.1016/j.scitotenv.2013.11.102

Polissar, A.V., Hopke., P.K., Harris., J.M. (2001). Source regions for atmospheric aerosol measured at Barrow, Alaska. Environ. Sci. Technol. 35, 4214–4226. https://doi.org/10.1021/es0107529

Ramanathan, V., Carmichael, G. (2008). Global and regional climate changes due to black carbon. Nat. Geosci. 1, 221–227. https://doi.org/10.1038/ngeo156

Ren, B. (2022). Speech at symposium on ecological protection and high-quality development in the Yellow River Basin. Frontiers 6, 91–96. https://doi.org/10.16619/j.cnki.rmltxsqy.2022.06.010 (in Chinese)

Shandong Provincial Bureau of Statistics (2022). Shandong Statistical Yearbook. China Statistics Press, China. http://tjj.shandong.gov.cn/tjnj/nj2022/zk/zk/indexce.htm

Tie, X., Geng, F., Guenther, A., Cao, J., Greenberg, J., Zhang, R., Apel, E., Li, G., Weinheimer, A., Chen, J., Cai, C. (2013). Megacity impacts on regional ozone formation: observations and WRF-Chem modeling for the MIRAGE-Shanghai field campaign. Atmos. Chem. Phys. 13, 5655–5669. https://doi.org/10.5194/acp-13-5655-2013

Tie, X., Zhang, Q., He, H., Cao, J., Han, S., Gao, Y., Li, X., Jia, X.C. (2015). A budget analysis of the formation of haze in Beijing. Atmos. Environ. 100, 25–36. https://doi.org/10.1016/j.atmosenv.2014.10.038

Wang, B., Liu, Z., Li, Z., Sun, Y., Wang, C., Zhu, C., Sun, L., Yang, N., Bai, G., Fan, G., Sun, X., Xia, Z., Pan, G., Xu, C., Yan, G. (2023a). Characteristics, chemical transformation and source apportionment of volatile organic compounds (VOCs) during wintertime at a suburban site in a provincial capital city, east China. Atmos. Environ. 298, 119621. https://doi.org/10.1016/j.atmosenv.2023.119621

Wang, Q., Wang, L., Tao, M., Chen, N., Lei, Y., Sun, Y., Xin, J., Li, T., Zhou, J., Liu, J., Ji, D., Wang, Y. (2021). Exploring the variation of black and brown carbon during COVID-19 lockdown in megacity Wuhan and its surrounding cities, China. Sci. Total Environ. 791, 148226–148226. https://doi.org/10.1016/j.scitotenv.2021.148226

Wang, Y., Ju, Q., Xing, Z., Zhao, J., Guo, S., Li, F., Du, K. (2023b). Observation of black carbon in Northern China in winter of 2018–2020 and its implications for black carbon mitigation. Sci. Total Environ. 877, 162897. https://doi.org/10.1016/j.scitotenv.2023.162897

Wang, Y.Q., Zhang, X.Y., Draxler, R.R. (2009). TrajStat: GIS-based software that uses various trajectory statistical analysis methods to identify potential sources from long-term air pollution measurement data. Environ. Modell. Software 24, 938–939. https://doi.org/10.1016/j.envsoft.2009.01.004

Xu, X., Akhtar, U.S. (2010). Identification of potential regional sources of atmospheric total gaseous mercury in Windsor, Ontario, Canada using hybrid receptor modeling. Atmos. Chem. Phys. 10, 7073–7083. https://doi.org/10.5194/acp-10-7073-2010

Yan, S., Gao, X., Pei, K., Sun, H., Wang, Y., Zhang, F., Li, Y., Wang, S., Chen, L., Dong, J., Yang, F. (2023). Mixing-layer depth-based backwards trajectory analysis of the sources of high O_3 concentrations at the Wutaishan station, North China. Atmos. Pollut. Res. 14, 101652. https://doi.org/10.1016/J.APR.2023.101652

Yan, Y., Zhuang, Q., Zan, C., Ren, J., Yang, L., Wen, Y., Zeng, S., Zhang, Q., Kong, L. (2021). Using the Google Earth Engine to rapidly monitor impacts of geohazards on ecological quality in highly susceptible areas. Ecol. Indic. 132, 108258. https://doi.org/10.1016/j.ecolind.2021.108258

Zhang, J., Liu, Q., Chen, L., Li, H., Zhao, R., Huang, X., Zhang, W., Wang, Y. (2022). Interannual evolution of elemental carbon-containing particles in winter in the atmosphere of Chengdu, China. Sci. Total Environ. 804, 150133–150133. https://doi.org/10.1016/j.scitotenv.2021.150133

Zhang, Q., Shen, Z., Zhang, T., Kong, S., Lei, Y., Wang, Q., Tao, J., Zhang, R., Wei, P., Wei, C., Cui, S., Cheng, T., Li, Z., Xu, H., Cao, J. (2020). Spatial distribution and sources of winter black carbon and brown carbon in six Chinese megacities. Sci. Total Environ. 762, 143075–143075. https://doi.org/10.1016/j.scitotenv.2020.143075

Zhang, Y., Tu, A., Zhang, W., Bian, Z., Wang, L. (2021). Variation characteristics and source analysis of black carbon aerosols in Huimin, Shandong. J. Mar. Meteorol. 41, 86–96. https://doi.org/10.19513/j.cnki.issn2096-3599.2021.02.009 (in Chinese)

Zhao, X.J., Zhao, P.S., Xu, J., Meng, W., Pu, W.W., Dong, F., He, D., Shi, Q.F. (2013). Analysis of a

winter regional haze event and its formation mechanism in the North China Plain. Atmos. Chem. Phys. 13, 5685–5696. https://doi.org/10.5194/acp-13-5685-2013

Zhao, T.L., Gong, S.L., Huang, P., Lavoué, D. (2012). Hemispheric transport and influence of meteorology on global aerosol climatology. Atmos. Chem. Phys. 12, 7609–7624. https://doi.org/10.5194/acp-12-7609-2012

Zheng, H., Kong, S., Wu, F., Cheng, Y., Niu, Z., Zheng, S., Yang, G., Yao, L., Yan, Q., Wu, J., Zheng, M., Chen, N., Xu, K., Yan, Y., Liu, D., Zhao, D., Zhao, T., Bai, Y., Li, S., Qi, S. (2019). Intra-regional transport of black carbon between the south edge of the North China Plain and central China during winter haze episodes. Atmos. Chem. Phys. 19, 4499–4516. https://doi.org/10.5194/acp-19-4499-2019

Zheng, H., Kong, S., Zheng, M., Yan, Y., Yao, L., Zheng, S., Yan, Q., Wu, J., Cheng, Y., Chen, N., Bai, Y., Zhao, T., Liu, D., Zhao, D., Qi, S. (2020). A 5.5-year observations of black carbon aerosol at a megacity in Central China: Levels, sources, and variation trends. Atmos. Environ. 232, 117581. https://doi.org/10.1016/j.atmosenv.2020.117581

Zhou, X., Gao, J., Wang, T., Wu, W., Wang, W. (2009). Measurement of black carbon aerosols near two Chinese megacities and the implications for improving emission inventories. Atmos. Environ. 43, 3918–3924. https://doi.org/10.1016/j.atmosenv.2009.04.062